

Graphene with time-dependent spin-orbit coupling: Truncated Magnus expansion approach

A. López¹, A. Scholz¹, Z. Z. Sun², and J. Schliemann¹

¹ Institute for Theoretical Physics, University of Regensburg, D-93040 Regensburg, Germany

² School of Physical Science and Technology, Soochow University, Suzhou, Jiangsu 215006, China

the date of receipt and acceptance should be inserted later

Abstract. We analyze the role of ac-driven Rashba spin-orbit coupling in monolayer graphene including a spin-dependent mass term. Using the Magnus expansion as a semi-analytical approximation scheme a full account of the quasienergy spectrum of spin states is given. We discuss the subtleties arising in correctly applying the Magnus expansion technique in order to determine the quasienergy spectrum. Comparison to the exact numerical solution gives appropriate boundaries to the validity of the Magnus expansion solution.

PACS. 81.05.ue Graphene – 71.70.Ej spin pumping, current driven – 72.25.Pn Spin-orbit coupling in condensed matter

1 Introduction

Typically, the dynamics of time-periodically driven systems is solved by means of Floquet's theorem.[1,2] A standard approach consists in performing a Fourier mode expansion of the eigenstates and then deal with the corresponding infinite dimensional eigenvalue problem by means of either numerical or approximate strategies to determine the so-called quasienergy spectrum. One alternative route which avoids the infinite dimensional eigenvalue formulation was put forward by Magnus [3,4] who proposed an exponential solution for the evolution operator given in terms of nested commutators of the time-dependent Hamiltonian. In a previous work [5] some of us have used the Magnus expansion (ME) in order to analyze the role of an ac-driven Rashba spin-orbit coupling (RSOC) on the spin dynamics of charge carriers in single layer graphene. However, as it was pointed out recently by Zhou and Wu [6], the reported results were beyond the convergence region of the ME solution. This in turn stems from the fact that within the Schrödinger picture representation, the convergence of the ME solution is momentum-dependent and, as a result, only valid for low momenta of the charge carriers. Indeed, in reference [6] it is shown that in the Schrödinger picture the ME solution is only valid within a small neighborhood of the Dirac point.

In the present paper we perform a thorough analysis of the subtleties arising when implementing the ME as a semi-analytical approach to the above quantum dynamics. As we shall see, switching from the Schrödinger to the interaction picture significantly improves the convergence

behavior.[7,8,9] This improvement, however, comes at a price: The Hamiltonian in the interaction picture is no longer time-periodic. As a consequence, the resulting time evolution operator in the Schrödinger representation arising from a *truncated* Magnus expansion does in general not fulfill the so-called stroboscopic property required from Floquet formalism.[1,2] However, as we shall see in the following, despite this shortcoming the results of the truncated analytical Magnus expansion performed in the interaction picture agree well with the exact numerics within the convergence range.

The paper is organized as follows. In section II we introduce the model Hamiltonian for periodically driven RSOC and present its exact analytical solution right at the Dirac point. The main results of the Floquet-Magnus approach for the semi-analytical solution of the evolution operator are presented in section III. Here, we also explore the ME for different bounds on the convergence domain reported in the literature. Next, in section IV we apply the ME approach to the driven RSOC problem at finite momentum, and compare with the exact numerical solution of the quasienergy spectrum. In section V we present a discussion of our main results. Finally, in section VI we give some concluding remarks and outlook.

2 Model

We consider a graphene monolayer being subject to a periodic time-dependent spin-orbit interaction of the (extrinsic) Rashba type. The sample is located on a certain substrate which induces a (mass) gap in the energy spectrum due to the intrinsic spin-orbit coupling. Thus, in Dirac

Correspondence to: alexander.lopez@physik.uni-regensburg.de

cone approximation, the system is described by the 4×4 Hamiltonian[10]

$$\mathcal{H}(\mathbf{p}, t) = v_F \boldsymbol{\sigma} \cdot \mathbf{p} + \Delta \sigma_z s_z + \lambda(t) \hat{z} \cdot [\boldsymbol{\sigma} \times \mathbf{s}], \quad (1)$$

where we have concentrated on the \mathbf{K} corner point of the Brillouin zone being the reference of the momentum \mathbf{p} . The results for the \mathbf{K}' point are obtained by setting $p_x \rightarrow -p_x$. Here $v_F \sim 10^6$ m/s is the Fermi velocity and the Pauli matrix vectors $\boldsymbol{\sigma}$ and \mathbf{s} describe the sublattice degree of freedom and the electron spin, respectively. On the other hand, Δ parametrizes the intrinsic spin-orbit coupling and $\lambda(t)$ describes the time-dependent RSOC which can, in principle, be induced by capacitor plates parallel to the setup and coupled to an LC circuit. In what follows we assume a time dependence of the form $\lambda(t) = \lambda_R \cos \Omega t$, with $\Omega = 2\pi/T$ being the frequency and T the period of the driving field. In the following we set $\hbar = 1$.

Upon applying the transformation

$$U(\mathbf{p}) = \frac{1}{\sqrt{2}} \begin{pmatrix} e^{-i\phi} \cos \frac{\gamma}{2} & -e^{-i\phi} \sin \frac{\gamma}{2} & e^{-i\phi} \cos \frac{\gamma}{2} & -e^{-i\phi} \sin \frac{\gamma}{2} \\ \sin \frac{\gamma}{2} & \cos \frac{\gamma}{2} & \sin \frac{\gamma}{2} & \cos \frac{\gamma}{2} \\ i \sin \frac{\gamma}{2} & i \cos \frac{\gamma}{2} & -i \sin \frac{\gamma}{2} & -i \cos \frac{\gamma}{2} \\ ie^{i\phi} \cos \frac{\gamma}{2} & -ie^{i\phi} \sin \frac{\gamma}{2} & -ie^{i\phi} \cos \frac{\gamma}{2} & ie^{i\phi} \sin \frac{\gamma}{2} \end{pmatrix}, \quad (2)$$

with $\tan \phi = p_y/p_x$ and $\tan \gamma = v_F p/\Delta$, the time-dependent Hamiltonian (1) becomes block-diagonal

$$\mathcal{H}(p, t) = \begin{pmatrix} H_-(p, t) & 0 \\ 0 & H_+(p, t) \end{pmatrix}, \quad (3)$$

where

$$H_{\pm}(p, t) = \pm \lambda(t) \sigma_0 + \frac{\Omega_0}{2} \sigma_z \mp \lambda(t) [\cos \gamma \sigma_z - \sin \gamma \sigma_x], \quad (4)$$

with $\Omega_0 = 2\sqrt{(v_F p)^2 + \Delta^2}$ and σ_0 being the 2×2 unit matrix. The transformation (2) can be constructed by first diagonalizing (1) at $\lambda = 0$ and expressing the full Hamiltonian in that eigenbasis. A further elementary transformation (diagonalizing the diagonal 2×2 blocks of the resulting Hamiltonian matrix) then leads to the basis encoded in (2). This result simplifies (but is equivalent to) the approach given previously in Ref. [5] in that it avoids explicit reference to an initial time.

Since both subblocks just differ in the sign of λ we focus on $H_+(p, t) \equiv H_S(p, t)$ and treat this time-periodic Hamiltonian via the Floquet theorem.[1,2] It states that the general solution of the dynamics can be written as

$$U(t) = P(t) e^{-iH_F t}, \quad (5)$$

with $P(t)$ being a periodic and H_F a constant matrix. The time evolution operator in (5) satisfies the stroboscopic property

$$U(nT) = P(nT) e^{-inTH_F} = [U(T)]^n. \quad (6)$$

The eigenvalues of H_F determine the quasienergy spectrum of the periodically driven problem.

First let us note that an exact solution for the spin dynamics generated by $H_S(p, t)$ can be found at $p = 0$ where the time evolution operator explicitly reads

$$U(t) = \mathcal{P}(t) e^{-i\Delta t \sigma_z}, \quad (7)$$

with $\mathcal{P}(t) = e^{-i(\sigma_0 - \sigma_z) f(t)}$ and we have defined

$$f(t) = \int_0^t \lambda(t') dt'. \quad (8)$$

Here, the quasienergy spectrum (modulo Ω) is given by

$$\varepsilon_{\pm}(p=0) = \pm \Delta. \quad (9)$$

At finite momentum the evolution operator admits, to the best of our knowledge, no analytical solution. A standard approach is to expand the solutions in an appropriately truncated basis of Fourier modes and to numerically diagonalize the resulting hermitian matrix. A semi-analytical alternative to this procedure will be discussed now.

3 Magnus expansion: General

Contrary to the numerical Fourier-Floquet solution, the Magnus expansion (ME) approach [3,4] avoids the diagonalization of a truncated eigenvalue problem, and similarly to the Fourier mode expansion approach it also has the physical virtue of preserving unitarity of the time evolution to any order in the expansion. This has to be contrasted to the approximate solution obtained through the Dyson series, where truncation at any given order leads to a non-unitary evolution. Although the Dyson series expansion always converges for bounded dynamical generators,[11] this is in general not true for the Magnus series. Thus, our next task is to summarize the most relevant subtleties that arise concerning the convergence of the Magnus series. These convergence restrictions will be important for the application of the ME strategy to the RSOC driven problem that is presented in the next section. For a more detailed and general discussion we refer the reader to reference [4].

Following Magnus [3], the time-evolution operator generated by the Schrödinger equation

$$i\partial_{\tau} U(\tau) = H(\tau) U(\tau). \quad (10)$$

(with $\tau = \Omega t$ and $H(\tau) = H_S(\tau)/\Omega$) can be formulated as

$$U(\tau) = e^{-iM(\tau)}, \quad (11)$$

where the exponent $M(\tau)$ is expressed as an infinite series

$$M(\tau) = \sum_{j=1}^{\infty} M_j(\tau). \quad (12)$$

The term $M_j(\tau)$ in this expansion is given in terms of integrals over sums of nested commutators with the first

contributions reading as

$$\begin{aligned}
M_1(\tau) &= \int_0^\tau H(\tau_1) d\tau_1 \\
M_2(\tau) &= \frac{1}{2} \int_0^\tau d\tau_1 \int_0^{\tau_1} [H(\tau_1), H(\tau_2)] d\tau_2 \\
M_3(\tau) &= \frac{1}{6} \int_0^\tau d\tau_1 \int_0^{\tau_1} d\tau_2 \int_0^{\tau_2} ([H(\tau_1), [H(\tau_2), H(\tau_3)]] \\
&\quad + [H(\tau_3), [H(\tau_2), H(\tau_1)]]) d\tau_3 \\
&\vdots
\end{aligned}$$

A key question regarding this approach is of course the convergence of the series (12). In his original work, Magnus gave an *a posteriori* convergence criterion in terms of the eigenvalues of the resulting operator M given in Eq. (11). However, for practical use *a priori* criteria dealing directly with the Hamiltonian appear also desirable. In general, the ME should not be expected to converge unless H is small in a suitable sense compared to the other typical energy scales in the problem. Specifically, bounds of the form

$$\int_0^\tau d\tau_1 \|H(\tau_1)\|_2 < r \quad (13)$$

have been investigated as convergence conditions, where $\|H\|_2$ is the euclidean norm of H defined as the squared root of the largest eigenvalue of the positive semi-definite operator $H^\dagger H$. The convergence radius r in the above inequality restricts the times $\tau' \in [0, \tau]$ for which the ME is applicable. The task of estimating r has a long history in the literature [12, 13, 14, 15]. Finally, it was established that a sufficient criterion for the convergence of the Magnus expansion is given by [16, 17]

$$\int_0^\tau d\tau_1 \|H(\tau_1)\|_2 < \pi. \quad (14)$$

To get an insight into the meaning of this convergence boundary we summarize the analysis given in **lemma 3** of reference [4] where it is established that the critical value $r_c = \pi$ arises from the evaluation of the poles of the derivative of the inverse exponential function, which is the Magnus expansion. These poles are given as $2mi$ with $m = \pm 1, \pm 2, \dots$, from which one gets the lowest value $r_c = \pi$. Moreover, the above value $r_c = \pi$ was shown to be sharp in the sense that it cannot be enlarged without further assumptions on the Hamiltonian. [17]

In the following section we apply the convergence restriction (14) in order to determine the most suitable parameter values that allow a semi-analytical description of the quasienergy spectrum for the RSOC driven setup.

4 Magnus expansion: Application

Let us first explore the criterion (14) in the Schrödinger picture of quantum dynamics used so far. Defining $\kappa = v_F p / \Omega$, $\Lambda = \lambda_R / \Omega$, and $\delta = \Delta / \Omega$ the inequality (14)

$$\int_0^\tau \sqrt{\kappa^2 + [\Lambda \cos \tau_1 - \delta]^2} d\tau_1 < \pi \quad (15)$$

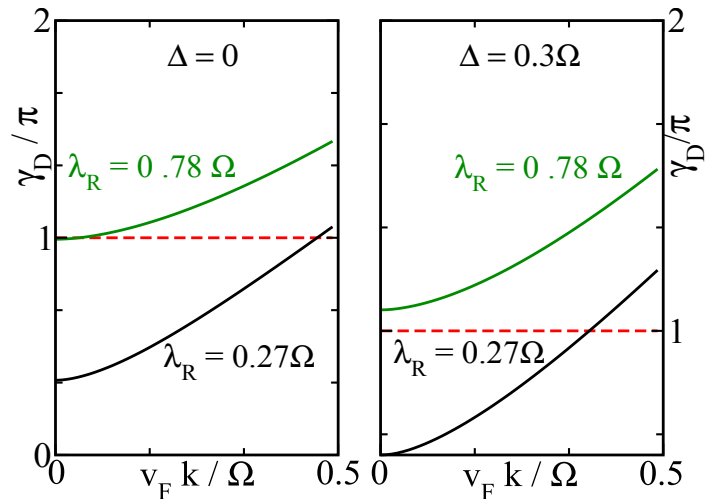


Fig. 1. (Color online) Normalized one-period dynamical phase that is related to the convergence of the ME in the Schrödinger representation defined as the l.h.s of inequality (15) for $\tau = 2\pi/\Omega$. The data is shown as a function of wave vector for different Rashba coupling strength λ_R , with $\Delta = 0$ (left) and $\Delta = 0.3\Omega$ (right). The dotted red line is a guide to the eye corresponding to $\gamma = \pi$ in Eq. (15). Although the convergence domain grows with decreasing coupling parameters λ_R and Δ , the ME is, in the Schrödinger representation, typically applicable only in a rather small neighborhood of the Dirac point, and for large couplings the convergence domain indeed shrinks to zero.

limits the validity of the ME solution to rather small momenta (see below), as pointed out in Ref. [6] on the basis of explicit numerics. Another way to explore this issue is to consider the instantaneous eigenvalues of the time-dependent Hamiltonian,

$$E_{\pm}(\tau) = \pm \sqrt{\kappa^2 + [\Lambda(\tau) - \delta]^2}, \quad (16)$$

leading to an accumulated dynamical phase

$$\gamma_D^{\pm} = \pm \int_0^{2\pi} d\tau \sqrt{\kappa^2 + [\Lambda(\tau) - \delta]^2}. \quad (17)$$

in a full period (with a vanishing Berry phase). The modulus of this expression is precisely the l.h.s of the convergence criterion (14) and is plotted in figure 1. As seen there, the applicability of the ME in the Schrödinger picture is limited to rather small momenta. This finding is indeed similar to earlier observations by Salzman. [18]

A qualitative improvement is achieved by changing to the interaction picture. Defining the “unperturbed” Hamiltonian H_0 to be that diagonal part of $H_+(t)$ given in Eq. (4) that has only a trivial time dependent term proportional to the unit matrix, the effective “perturbation” $V = H - H_0$ reads in the interaction picture

$$V_I(\kappa, \tau) = \Lambda \cos(\tau) \begin{pmatrix} -\cos \gamma & \sin \gamma e^{i\omega_0 \tau} \\ \sin \gamma e^{-i\omega_0 \tau} & \cos \gamma \end{pmatrix}, \quad (18)$$

with $\omega_0 = 2\sqrt{\kappa^2 + \delta^2}$ and $\tan \gamma = \kappa/\delta$. In this representation, the convergence radius of the Magnus solution be-

comes momentum-independent and restricts the effective coupling constant Λ by the inequality

$$\Lambda \int_0^\tau |\cos \tau_1| d\tau_1 < \pi. \quad (19)$$

Evaluation after one period gives the numerical restriction $\Lambda_1 < \pi/4 \approx 0.78$, whereas the extension to larger time domains reduces the coupling constant as $\Lambda_n < \Lambda_1/n$. Hence, it is important to notice that in order to correctly apply the ME the restriction (19) must always be fulfilled. Although switching to the interaction representation improves the convergence of the ME, the dynamical equations

$$i\partial_\tau U_I(\tau) = V_I(\tau)U_I(\tau) \quad (20)$$

are not longer generated by a periodic operator since $V_I(\tau + 2n\pi) \neq V_I(\tau)$. Thus, Floquet's theorem does not apply and no stroboscopic evolution will follow for $U_I(\tau)$. On the other hand, the full time evolution operator in the Schrödinger picture

$$U(\tau) = e^{if(\tau)} e^{-i\omega_0\tau\sigma_z/2} U_I(\tau) \quad (21)$$

with $U_I(\tau)$ evaluated by the full (i.e., untruncated) ME of course obeys the stroboscopic condition (6) provided the ME converges. In practical calculations, however, it is usually (as well as in the present case here) not possible to evaluate all terms of the ME, and one truncates this series at rather low order.

In order to compute the quasienergy spectrum from the time evolution operator $U(\tau)$ without making use of the stroboscopic relation (6), one needs to calculate the logarithm of $U(nT)$ for some integer n . The difficulty here is that the complex logarithm is not a single-valued function, and for different n the results may lie on different sheets. Unfortunately, it is impossible to properly keep track of these phases without prior knowledge of the quasienergies which are in fact supposed to be the results of this computational step. Such difficulties do not arise for $n = \pm 1$ since the division by n has only a trivial effect here, and it is easy to see that a move to another sheet of the complex logarithm is just a shift to another periodicity interval of quasienergies. Regarding general n , there are only very special cases where $U(nT)$ can be calculated in such an explicit fashion that one can immediately read off the quasienergies. As an example, consider $\gamma = \pi/2$ ($\Leftrightarrow \delta = \Delta = 0$) at resonance $\kappa = \kappa_{res} = \pi$ ($\Leftrightarrow k = \Omega/2v_F$). Here the computational complexity is significantly reduced, and one finds in first-order ME

$$U(\kappa_{res}, nT) = \exp \left\{ -i \left(\frac{\lambda_R}{2} \sigma_x + \frac{\Omega}{2} \right) nT \right\} \quad (22)$$

with the quasienergies $\varepsilon_\pm = \Omega/2 \pm \lambda_R/2$. This result obtained for general n relies on the possibility to write $U(nT)$ explicitly as a single exponential whose argument is linear in n . Unfortunately, such a situation arises only in particular cases. Another example is of course the case $k = 0$ already discussed in section 2.

Following the above discussion, we will therefore concentrate on the case $n = 1$ when evaluating the time evolution. As we shall see, this procedure leads to accurate approximations to the quasienergy spectrum. Since the interaction $V_I(\tau)$ is a 2×2 matrix we can write $M(\tau) = \mathbf{m}(\tau) \cdot \boldsymbol{\sigma}$, and the Magnus series amounts to write the vector series

$$\mathbf{m}(\tau) = \mathbf{m}_1(\tau) + \mathbf{m}_2(\tau) + \dots, \quad (23)$$

where the j th vector contribution is of order Λ^j and is obtained by integration of nested commutators of the interaction term. The evolution operator in the interaction picture can be written as

$$U_I(\tau) = \cos |\mathbf{m}(\tau)| - i \text{sinc} |\mathbf{m}(\tau)| \mathbf{m}(\tau) \cdot \boldsymbol{\sigma}, \quad (24)$$

where $\text{sinc}(x) = \sin(x)/x$ and $|\mathbf{m}(\tau)|$ is the norm of the vector $\mathbf{m}(\tau)$. Using expression (24), the evolution operator in the Schrödinger picture Eq. (21) becomes

$$U(\tau) = e^{if(\tau)} [u_0(\tau) - i\mathbf{u}(\tau) \cdot \boldsymbol{\sigma}], \quad (25)$$

where $f(\tau)$ is defined in equation (8) and $u_0(\tau)$ as well as the components of the time-dependent vector $\mathbf{u}(\tau) = (u_x(\tau), u_y(\tau), u_z(\tau))$ read

$$\begin{aligned} u_0(\tau) &= \cos \frac{\omega_0\tau}{2} \cos |\mathbf{m}(\tau)| - m_z(\tau) \sin \frac{\omega_0\tau}{2} \text{sinc} |\mathbf{m}(\tau)| \\ u_x(\tau) &= \text{sinc} |\mathbf{m}(\tau)| \left[m_x(\tau) \cos \frac{\omega_0\tau}{2} - m_y(\tau) \sin \frac{\omega_0\tau}{2} \right] \\ u_y(\tau) &= \text{sinc} |\mathbf{m}(\tau)| \left[m_y(\tau) \cos \frac{\omega_0\tau}{2} + m_x(\tau) \sin \frac{\omega_0\tau}{2} \right] \\ u_z(\tau) &= m_z(\tau) \text{sinc} |\mathbf{m}(\tau)| \cos \frac{\omega_0\tau}{2} + \sin \frac{\omega_0\tau}{2} \cos |\mathbf{m}(\tau)|. \end{aligned} \quad (26)$$

From the unitarity of (25), the quasienergies $\varepsilon_\pm(\kappa)$ are then given by

$$\varepsilon_\pm(\kappa) = \pm \frac{1}{2\pi} \tan^{-1} \left(\frac{\sqrt{1 - u_0^2(\kappa, 2\pi)}}{u_0(\kappa, 2\pi)} \right), \quad (27)$$

where we have again made explicit the momentum dependence. Therefore, the calculation of the quasienergy spectrum reduces to finding $u_0(2\pi)$, which in turn amounts to calculate both $|\mathbf{m}(2\pi)|$ and $m_z(2\pi)$. However it is important to point out that for studying the dynamical behavior of any physical quantity of interest all the equations (26) need to be solved. In the following we use the notation ε_j to denote the approximate quasienergy spectrum obtained by means of a j -order truncation of the ME. To first-order, the components of the vector $\mathbf{m}(\tau)$ are found by integration of equation (18) which leads to

$$\begin{aligned} m_x(\tau) &= \frac{\Lambda \sin \gamma}{2} \left(\frac{\sin \omega_+\tau}{\omega_+} + \frac{\sin \omega_-\tau}{\omega_-} \right) \\ m_y(\tau) &= \frac{\Lambda \sin \gamma}{2} \left(\frac{1 - \cos \omega_+\tau}{\omega_+} + \frac{1 - \cos \omega_-\tau}{\omega_-} \right) \\ m_z(\tau) &= -\Lambda \cos \gamma \sin \tau. \end{aligned} \quad (28)$$

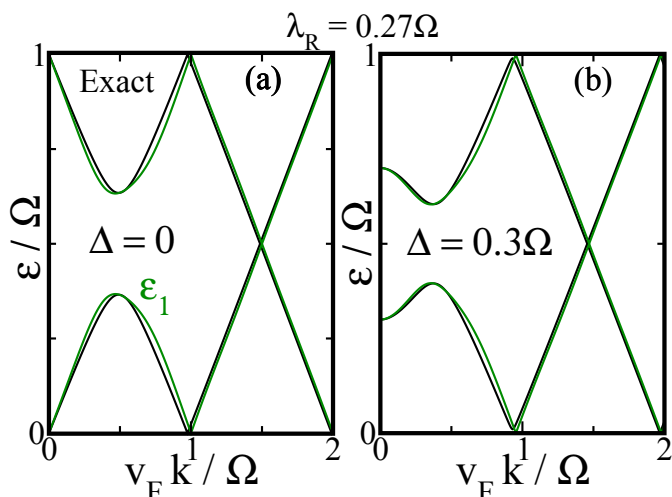


Fig. 2. (Color online) The quasienergy spectra obtained by means of an exact numerical diagonalization (black line) and the first-order ME approximation (green line) evaluated at $\lambda_R = 0.27\Omega$, well below the boundary value derived from the convergence condition reported in reference. [17] Fixing Ω as energy scale one finds good qualitative and quantitative agreement between the first-order ME and the numerical exact solutions within one period as shown in panel a (b) for vanishing (finite) intrinsic spin-orbit contribution Δ .

In order to simplify the notation we have introduced the shifted frequencies $\omega_{\pm} = \omega_0 \pm 1$. Notice that for $\tau = 2\pi$, the component $m_z(\tau)$ vanishes. Therefore, the modulus $m(2\pi) \equiv m$ becomes

$$m = \frac{4\pi\Lambda\kappa}{\omega_+} |\text{sinc}(\pi\omega_-)|. \quad (29)$$

and we get to first-order in the interaction strength

$$\varepsilon_{\pm}(\kappa) = \pm \frac{1}{2\pi} \tan^{-1} \left(\frac{\sqrt{1 - \cos^2 \pi\omega_0 \cos^2 m}}{\cos \pi\omega_0 \cos m} \right), \quad (30)$$

whereas taking into account the second-order contributions leads to rather lengthier expressions since now we have $|m(2\pi)| = \sqrt{m_z^2 + m_{\parallel}^2}$, with

$$|m_{\parallel}| = 4\Lambda\kappa \left| \frac{\pi \text{sinc}(\pi\omega_-)}{\omega_+} - \frac{2\Lambda\delta \text{sinc}(\pi\omega_0)}{\omega_0(\omega_0^2 - 4)} \right|$$

$$m_z = \frac{4\Lambda^2\kappa^2}{\omega_+\omega_-} \left[\frac{\pi}{\omega_0} - \frac{\sin(2\pi\omega_0)}{\omega_+\omega_-} \right]. \quad (31)$$

In the appendix we summarize the results for the contributions to the ME up to the third-order. In figure 2 we show the first-order ME quasienergy spectrum corresponding to $\lambda_R = 0.27\Omega$ (i.e., well below the critical value $\lambda_R = 0.78\Omega$). Panel a (b) shows the result for zero (finite) intrinsic spin-orbit contribution. In both panels of figure 2 the green line corresponds to the first-order ME whereas

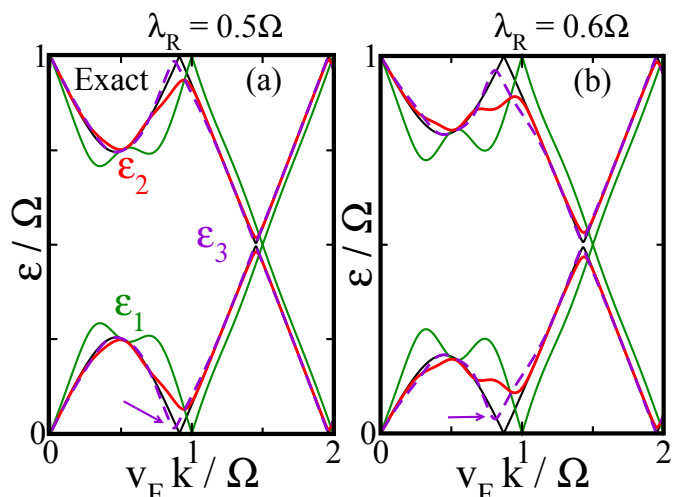


Fig. 3. (Color online) Quasi-energy spectra for exact (black, continuous line), first (green, continuous line), second (red, continuous line) and third (violet, dashed line) ME solutions for vanishing $\delta = 0$ mass term. In this strong coupling regime with values of the effective coupling amplitude below the one given by the convergence criteria $\lambda_R = 0.78\Omega$ reported in [16,17] the third-order ME fits very well the exact result (see discussion in the main text).

the black line is the result from the exact numerical diagonalization. Thus, for this small coupling we see that even the first-order ME solution fits qualitatively and quantitatively well the results from the exact numerical solution and describes properly the gap opening at finite momenta reported in references [19,20,21], with the largest gap located at $\omega_0 = 1/2$. To approach the convergence bound $\lambda_R = 0.78\Omega$, higher order contributions to the ME need to be included. This is shown in figure 3 where we present the exact numerical solution (black continuous) along with the first (green, continuous line), second (red, continuous line) and third (violet, dashed line) order one-period ME approximation for $\lambda_R = 0.5\Omega$ (a) and $\lambda_R = 0.6\Omega$ (b). As the convergence is not changed by Δ we restrict ourselves, without loss of generality, to the case $\Delta = 0$. From panel (a) in 3 we find that up to $\lambda_R = 0.5\Omega$ only third-order ME fits well the numerically exact solution, with minor deviations in the vicinity of the zero of the exact solution. This zero of the quasienergies appears in the vicinity of $v_F k = \Omega$. As it is depicted by the arrows, this discrepancy is more noticeable in panel (b).

On the other hand, in panel (a) of figure 4 we explore the RSO coupling regime at the boundary $\lambda_R = 0.78\Omega$ whereas in panel (b) we set $\lambda_R = \Omega$, i.e., beyond the convergence domain. In the left panel we notice that even at the convergence boundary the truncated ME solution ε_3 (violet, continuous line) does not properly describe the locations of the gap openings from the exact solution (black, continuous line), and also shows a wavelike behavior indicating that more terms are needed to get a better approximation. This is a consequence of the perturbative nature of the approach. Still, we find that the ME solution qual-

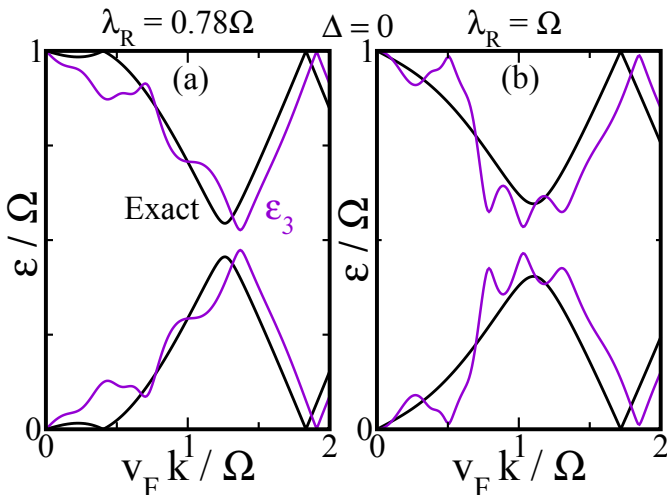


Fig. 4. (Color online) Quasi-energy spectra for exact (black line) and third-order (violet line) ME solutions, for vanishing ($\delta = 0$) mass term. We notice that at $\lambda_R = 0.78\Omega$ the third-order ME considerably deviates from the exact result as more terms in the perturbative expansion are required to fit the exact solution. However, at larger $\lambda_R = \Omega$ (panel b), the ME does not converge and addition of more terms would not improve the approximated quasienergy spectrum.

itatively “follows” the exact solution. For coupling values beyond the convergence bound (right panel) the discrepancies are more obvious because even the full ME solution breaks down. In contradistinction to the improvements resulting from adding of more terms to the ME, due to the convergence restriction, the coupling regime $\lambda_R > 0.78\Omega$ is not suitable to be treated by means of the ME approach.

Although the convergence restriction restrains the applicability of the ME it is important to remark that one of its main advantages over the numerical Fourier-mode counterpart is that we can get valuable analytical information on the momentum dependence of the gaps by just finding the maxima of the first-period quasienergy $\varepsilon_+ \equiv \varepsilon(\kappa)$. For instance, within the low coupling limit the first-order ME expressions given in equation Eq. (27) appropriately gives the expected result for the gaps at $2\kappa = 1$. Yet, we notice in panel (a) of figure 4 that for large values of the coupling constant, the gap is noticeable shifted from $2\kappa = 1$. Its behavior is obtained from the maxima of

$$\varepsilon(\kappa) = \frac{1}{2\pi} \tan^{-1} \left(\frac{\sqrt{1 - u_0^2(\kappa)}}{u_0(\kappa)} \right), \quad (32)$$

that leads to the following expressions

$$\left(\frac{2u_0^2 - 1}{\sqrt{1 - u_0^2}} \right) \frac{\partial u_0}{\partial \kappa} = 0, \\ \frac{1}{2\pi} \left[\frac{u_0[1 + 2(1 - u_0^2)]}{(1 - u_0^2)^{3/2}} \left(\frac{\partial u_0}{\partial \kappa} \right)^2 + \frac{2u_0^2 - 1}{\sqrt{1 - u_0^2}} \frac{\partial^2 u_0}{\partial \kappa^2} \right] < 0,$$

where, to simplify the notation, we have set $u_0(\kappa, 2\pi) = u_0$. The first relation implies either $u_0^2 = 1/2$ and/or $\frac{\partial u_0}{\partial \kappa} = 0$. However, substitution of $u_0^2 = 1/2$ on the second condition leads to the contradiction $(2\frac{\partial u_0}{\partial \kappa})^2 < 0$. Then, the maxima are found from the (in principle) simplified conditions $\frac{\partial u_0}{\partial \kappa} = 0$, $\frac{\partial^2 u_0}{\partial \kappa^2} < 0$.

5 Discussion

The fact that changing to the interaction representation improves the convergence of the ME is certainly not a peculiarity of the model considered here. For example, Pechukas and Light[14] showed that this is also true for the paradigmatic example of a driven quantum harmonic oscillator. In particular, for the linearly driven quantum harmonic oscillator the ME terminates at second-order, and thus no truncation is necessary. Hence, only convergence issues have to be dealt with. In addition, for a two-level driven problem the same authors show that the m -th order ME solution gives a more accurate description of the dynamics than perturbation theory to the same order of approximation. This higher degree of accuracy is associated to the unitarity preserving property of the ME approach. Salzman[22] and Fernandez[23] also deal with the driven quantum harmonic oscillator and conclude that the ME solution will always converge for times within the first period $0 < t < T$. This problem admits an exact analytical solution and the authors show that the ME solution gives a proper account of the dynamics apart for values of the driving frequency near resonances. Our results indicate that, within its convergence domain, the truncated ME provides a suitable description of the dynamical behavior of physical quantities within the time window $0 < t < T$. However, due to the momentum independence of the restriction $\lambda_R = 0.78\Omega$, we found that intermediate values of the coupling ($0.5\Omega \leq \lambda_R \leq 0.6\Omega$), the quasienergy spectrum is properly described even at resonances by the third-order truncated ME. Concerning energy scales the value of the intrinsic and extrinsic spin-orbit coupling parameters Δ and λ_R in graphene have been obtained by tight binding [24] and first principle calculations [25,26]. They gave estimates in the range $10^{-6} - 10^{-5}$ eV, much smaller than any other energy scale in the problem (kinetic, interaction and disorder). However, the RSOC strength has recently been reported[27] from the band splitting to be of order $2\lambda_R \approx 225$ meV. Using this value and the boundary (in full dimensional form) $2\lambda_R = \pi\hbar\Omega/2$ and putting $\Omega = 2\pi\nu$ we get the corresponding frequency to be $\nu \approx 35$ THz. In addition, we have seen that comparing the semi-analytical to the exact numerical approach a key feature of the dynamical description by means of the truncated ME approach is that explicit formulae are obtained for the quasienergy spectrum. Therefore, the analysis of the gap openings in the low and intermediate coupling regime can be given a semi-analytical treatment. This feature might provide useful information on the underlying physical processes leading to a better understanding of the nature of these

important features of the quasienergy spectrum in more complicated setups.

6 Conclusions

In this work we have described semi-analytically the quasienergy spectrum of charge carriers in graphene under ac-driven RSOC interaction by means of the ME approach. We have shown that within the Schrödinger picture the ME is only applicable within a small neighborhood of the Dirac point and makes it non suitable to describe the induced gap openings at finite momenta. This difficulty is overcome by changing to the interaction picture where the convergence domain becomes momentum independent and just restricts the effective coupling to values $\lambda_R \leq 0.78\Omega$. Although using this formulation the truncated ME evolution operator violates the stroboscopic property, we found that for low values of the coupling constant the truncated first-order ME solution fits very well the exact quasienergy spectrum. In addition, for values of the coupling constant up to $\lambda_R = 0.5\Omega$ the spectrum is properly described by the third-order ME solution. Evaluation at the boundary $\lambda_R = 0.78\Omega$ shows the need to include more terms, whereas for values such as $\lambda_R = \Omega$ the Magnus approximation breaks down. As shown in previous works[8,22] the ME always converges in $0 < t < T$, and therefore our results for the one-period quasienergy spectrum are in agreement with these previous reports. In contrast to its numerical counterparts, one of the key features of the ME approach is that its analytical nature allows the determination of the momentum dependence of the gaps from which valuable information on the position of the resonant processes can be obtained. In summary, we have shown that implementation of the ME approach provides a valuable tool to get physical insight into the mean features of a driven problem and it would shed light on the description of more complicated driven problems, provided good care is paid on determining the appropriate parameter ranges as we have discussed.

Acknowledgments. We thank M. W. Wu and Y. Zhou for useful correspondence. A. L. Acknowledges fruitful discussions with B. Santos. This work has been supported by Deutsche Forschungsgemeinschaft via GRK 1570.

Appendix

Derivation of second and third-order contributions to the ME in the interaction picture

The adimensional dynamical generator in the interaction picture is written in terms of the Pauli matrices as

$$V_I(\tau) = \Lambda \cos \tau \left[\sin \gamma (\cos \omega_0 \tau \sigma_x - \sin \omega_0 \tau \sigma_y) - \cos \gamma \sigma_z \right]. \quad (33)$$

Using the simplifying notation $V_I(\tau_j) = V_j$, and denoting the second and third-order contribution to the ME

respectively as M_2 and M_3 , one has

$$\begin{aligned} M_2(\tau) &= \frac{-i^2}{2} \int_0^\tau d\tau_1 \int_0^{\tau_1} [V_1, V_2] d\tau_2 \\ M_3(\tau) &= \frac{-i^3}{6} \int_0^\tau d\tau_1 \int_0^{\tau_1} d\tau_2 \int_0^{\tau_2} \left([V_1, [V_2, V_3]] \right. \\ &\quad \left. + [V_3, [V_2, V_1]] \right) d\tau_3. \end{aligned} \quad (34)$$

Performing the integrations, and evaluating at one period, i.e. $\tau = 2\pi$, we obtain for the second-order ME term the result

$$\begin{aligned} M_2(2\pi) &= \frac{\Lambda^2}{2(\omega_0^2 - 4)(\omega_0^2 - 1)^2} \left\{ 4 \sin 2\gamma \sin \pi \omega_0 \right. \\ &\quad \times (\sigma_x \cos \pi \omega_0 - \sigma_y \sin \pi \omega_0) (\omega_0^2 - 1)^2 \\ &\quad \left. - \omega_0 \sigma_z \left[\pi (\omega_0^2 - 1) - \omega_0 \sin 2\pi \omega_0 \right] \right. \\ &\quad \left. \times (\omega_0^2 - 4) (1 - \cos 2\gamma) \right\}. \end{aligned} \quad (35)$$

Therefore, to second order we get now a finite σ_z component that shifts the zeroes of the quasienergy spectrum as shown in figures 3 and 4. From this expression we explicitly see the appearance of another resonance at $\Omega = 2\Omega_0$, in addition to that corresponding to $\Omega = \Omega_0$, which is properly described by the first-order ME solution as it was explicitly worked out in section IV. This additional resonant contribution weights the higher momentum gap openings that are shown in figures 2-3, yet they are small in amplitude as compared to the one-photon resonance leading to the largest gap opening. This is in agreement with the Fourier-mode expansion solution for moderate values of the effective coupling strength Λ .

In order to use the ME solution for values close to the convergence boundary given by *Casas*,[17] we have also evaluated the first-period third-order contribution to the ME. After integration up to the first period one finds in this case the results

$$\begin{aligned} M_3(2\pi) &= \frac{\Lambda^3 \omega_0 \sin \gamma}{6(\omega_0^2 - 1)^3 (\omega_0^2 - 4) (\omega_0^2 - 9)} \\ &\quad \times \left\{ 12 \sin 2\gamma \sin 2\pi \omega_0 (\omega_0^2 - 9) (\omega_0^2 - 1)^2 \sigma_z \right. \\ &\quad \left. + (\sigma_x \cos \pi \omega_0 - \sigma_y \sin \pi \omega_0) (\omega_0^2 - 4) \right. \\ &\quad \times \left[\omega_0 \cos 2\gamma (3\omega_0 \sin \pi \omega_0 (2 + 11(3 - \omega_0^2))) \right. \\ &\quad \left. + (\omega_0^2 - 9) (6\pi \cos \pi \omega_0 (\omega_0^2 - 1) - \omega_0 \sin 3\pi \omega_0) \right) \\ &\quad \left. - (\omega_0^2 - 9) (6\pi \cos \pi \omega_0 (\omega_0^2 - 1) - \omega_0^2 \sin 3\pi \omega_0) \right) \\ &\quad \left. - 3 \sin \pi \omega_0 (16 + 3\omega_0^2 + 5\omega_0^4) \right\}, \end{aligned} \quad (36)$$

which, as expected, contains higher order photon resonant contributions. Continuing this perturbative treatment, larger domains of values the coupling strength are reachable but the addition of higher order terms lead to rather lengthier expressions and go beyond the main focus of the present work.

References

1. M. Grifoni and P. Hänggi, *Physics Reports* **304**, 229 (1998)
2. S.-I Chu and D. A. Telnov, *Physics reports* **390**, 1 (2004)
3. W. Magnus, *Commun. Pure Applied Math.* **VII**, 649673 (1954)
4. S. Blanes, F. Casas, J. A. Oteo, and J. Ros, *Physics reports* **470**, 151 (2009)
5. A. Lopez, Z. Z. Sun and J. Schliemann, *Phys. Rev. B* **85**, 205428 (2012)
6. Y. Zhou and M. W. Wu, *cond-matt.mes-hall* 1206.4093 (2012)
7. E. B. Fel'dman, *Phys. Lett.* **104A**, 479 (1984)
8. F. M. Fernandez, *Phys. Rev. A* **41**, 2311 (1990)
9. E.S Mananga and T. Charpentier, *J. Chem. Phys.* **135**, 044109 (2011)
10. C. L. Kane and E. J. Mele, *Phys. Rev. Lett.* **95**, 226801 (2005)
11. J. A. Oteo and J. Ros, *J. Math. Phys.* **41**, 3268 (2000)
12. A. Agračhev and R. Gamkrelidze, *J. Sov. Math.* **17**, 1650 (1981)
13. P. A. Vela, *Averaging and Control of Nonlinear Systems*, PhD thesis, California Institute of Technology, (2003)
14. P. Pechukas and J. C. Light, *J. Chem. Phys.* **44**, 3897 (1966)
15. S. Blanes, F. Casas, J. A. Oteo and J. Ros, *J. Phys. A: Math. Gen.* **31**, 259 (1998)
16. Ch. Moan and J. Niesen, *Found. Comput. Math.* **8**, 291 (2008)
17. F. Casas, *J. Phys. A: Math. Theor.* **40**, 15001 (2007)
18. W. R. Salzman, *Phys. Rev. A* **36**, 5074 (1987)
19. T. Oka and H. Aoki, *Phys. Rev. B* **79**, 081406(R) (2009)
20. Y. Zhou and M. W. Wu, *Phys. Rev. B* **83**, 245436 (2011)
21. H. L. Calvo, H. M. Pastawski, S. Roche and L. E. F. Foa Torres, *Appl. Phys. Lett.* **98**, 232103 (2011)
22. W. R. Salzman, *J. Chem. Phys.* **85**, 4605 (1986)
23. F. Fernandez, *J. Chem. Phys.* **88**, 490 (1988)
24. H. Min, J. E. Hill, N. A. Sinitsyn, B. R. Sahu, L. Kleinman and A. H. MacDonald, *Phys. Rev. B* **74** 165310 (2006)
25. Y. Yao, F. Ye, X.-L. Qi, Z.-C. Zhang and Z. Fang, *Phys. Rev. B* **75**, 041401 (2007)
26. M. Gmitra, S. Konschuh, C. Ertler, C. Ambrosch-Draxl and J. Fabian, *Phys. Rev. B* **80** 235431 (2009)
27. Yu S. Dedkov, M. Fonin, U. Rüdiger and C. Laubschat, *Phys. Rev. Lett.* **100** 107602 (2008)